JOURNAL OF SOLID STATE CHEMISTRY 109, 265–271 (1994)

New Cluster Phases $A^IZr_6Cl_{14}Mn$ and $Zr_6Cl_{14}Fe$: A Second Structure Type with Small Cations

Jie Zhang and John D. Corbett[1]

Department of Chemistry, Iowa State University, Ames, Iowa 50011

Received May 5, 1993; accepted July 21, 1993

The new compounds $Zr_6Cl_{14}Z$, Z = Mn, Fe, and $AZr_6Cl_{14}Mn$, A = Li–Cs, have been synthesized by reactions of Zr, $ZrCl_4$, $MnCl_2$, or $FeCl_3$, and ACl where necessary in sealed Ta tubes at 750 to 850°C. All exist in stuffed versions of the orthorhombic Nb_6Cl_{14} (*Cmca*) structure. Single crystal studies were completed on $Zr_6Cl_{14}Fe$ and $LiZr_6Cl_{14}Mn$ (R_w = 5.5, 5.3%, respectively). The lithium cation occupies 25% of a set of distorted octahedral chlorine sites within the cluster network, in contrast to 12-coordinate site occupied by K, Rb, or Cs. The cations in $NaZr_6Cl_{14}Mn$ and $LiZr_6Cl_{14}B$ are also assigned to the octahedral site based on distinctive volume effects with small (or no) cations in both the Mn and B series.

INTRODUCTION

The intentional inclusion of "impurities" in the synthesis of reduced halides of zirconium has afforded a large family of new cluster phases with the general compositions $A_x^I[Zr_6(Z)X_{12}]X_n$, $0 \le x$, $n \le 6$ (1, 2). The interstitial atoms Z may range from hydrogen and the second period members Be–N through Al, Si, Ge, P to the transition metals Cr–Ni. The additional electronic variable supplied by Z coupled with those afforded by xA^+ cations and nX additional halides to bond at, or bridge between, zirconium vertexes in separate clusters is the principal factor that allows such a large variety of compounds and novel structures (3–10).

Although the iodides encapsulate a somewhat greater variety of Z, it is the chlorides (and bromides (11)) that give us the greater variety of structural choices as a function not only of composition (above) but also of the sizes of both A and the clusters. At the same time, the chlorides adhere better to the ideal closed shell electron counts of 14 with main group (s, p) Z (3) and 18 with transition metal Z (6). Only a few of the structure types found with zirconium were already known (without Z) in classical clusters of niobium and tantalum, the latter probably being limited by fairly stringent electronic and structural requirements in the absence of the versatility provided by Z. The most common of these is probably the orthorhombic Nb_6Cl_{14} member (12), which has been modified by the addition of A^I and Z in $AZr_6I_{14}Z$, A^I = Cs, Rb, or K, Z = B, C (3) and $AZr_6Cl_{14}Z$, A = Li–Cs or Tl for Z = B or, in a few cases, C (13). In each case, A^I is 12-coordinated by halide. However, an inexplicable result in the last study was an expansion of the unit cell of $Zr_6Cl_{14}B$ with A = Li but not heavier A. The present study extends the $AZr_6Cl_{14}Z$ examples to those encapsulating the transition metals Mn and Fe as well as provides the first identification of a second structure in which small A^I is bound in another site in the lattice framework.

EXPERIMENTAL SECTION

The quality of the starting materials, the syntheses of $ZrCl_4$, anhydrous $MnCl_2$ and $FeCl_3$, and powdered Zr, the reaction techniques utilizing welded Ta containers, and Guinier diffraction and analysis procedures have all been described before (10). All reactants and products were handled only in a high quality glove box. The phase distributions within/purities of products were in all cases estimated from their Guinier powder patterns.

Syntheses

The new Zr_6Cl_{14} (Nb_6Cl_{14}-type) compounds obtained are presented in Table 1 along with their lattice dimensions. Among the 18-electron cluster phases, $Zr_6Cl_{14}Fe$ and $A^IZr_6Cl_{14}Mn$ (A = K, Rb, Cs) could be obtained regularly in high yields from appropriate quantities of ACl, Zr, $ZrCl_4$, and ZCl_x at 800–850°C. These have also often been observed as side products coexisting with other cluster products when a reaction failed to give the target phases. A relatively high stability is implied. On the other hand, $LiZr_6Cl_{14}Mn$ could be synthesized as a single phase only around 750°C. At 850°C, the on-stoichiometry reaction instead produced $Li_2Zr_6Cl_{15}Mn$ (8) and ZrCl. Similarly, $NaZr_6Cl_{14}Mn$ was obtained at 800°C only in the

[1] To whom correspondence should be addressed.

0022-4596/94 $6.00

TABLE 1
Cell Parameters (Å) and Volumes (Å^3) of $AZr_6Cl_{14}Z$ Compounds[a]

Compound	a	b	c	V	Cation site[b]
$Zr_6Cl_{14}Mn$	14.486(2)	12.793(3)	11.803(2)	2187.2(7)	—
$LiZr_6Cl_{14}Mn$	14.507(2)	12.858(2)	11.786(2)	2198.5(5)	a
$NaZr_6Cl_{14}Mn$	14.478(6)	13.026(4)	11.752(4)	2216(1)	a
$KZr_6Cl_{14}Mn$	14.347(2)	12.838(2)	11.796(2)	2172.6(5)	b
$RbZr_6Cl_{14}Mn$	14.3451(8)	12.8444(8)	11.8453(6)	2182.5(2)	b
$CsZr_6Cl_{14}Mn$	14.381(1)	12.869(1)	11.933(1)	2208.5(3)	b
$Zr_6Cl_{14}Fe$	14.332(4)	12.772(4)	11.778(6)	2156(1)	—

[a] From Guinier powder diffraction data with Si as internal standard, $\lambda = 1.54056$ Å. Space group *Cmca*.
[b] *a* denotes the Li position in $LiZr_6Cl_{14}Mn$ (this work) and *b*, that for Cs in $CsZr_6I_{14}C$ (Ref. 3).

company of ZrCl plus other less reduced phases, but its yield was about 90% (plus ~10% of an unknown phase) at 750°C. The differences in the thermal stabilities that separate the 18-electron $A^1Zr_6Cl_{14}Mn$ compounds into two groups will be rationalized by their structural differences.

The 17-electron cluster $Zr_6Cl_{14}Mn$ was first observed following an attempt to synthesize $Zr_6Cl_{13}Mn$, a hypothetical 18-electron analogue of $Zr_6Cl_{13}B$ (14). However, the necessary expansion of the cluster core must introduce an instability in the less flexible target lattice sufficient to give a 17-electron cluster with the Nb_6Cl_{14} structure instead. The formation of $Zr_6Cl_{14}Mn$ is also sensitive to the reaction temperature; stoichiometric reactions at 800°C yield only noncluster phases such as $ZrCl_4$ and ZrCl, while $Zr_6Cl_{14}Mn$ is produced at 700°C.

The unidentified phase noted above in the $NaZr_6Cl_{14}Mn$ synthesis has been repeatedly observed and can be obtained as the principal product with a NaCl : $NaZr_6Cl_{14}Mn$ ratio of 5 : 1. It shows a large number of reflections in the low angle region of its powder pattern, and single crystals will doubtlessly be necessary to deduce its structure.

Structural Studies

Single crystal X-ray analyses were performed on $Zr_6Cl_{14}Fe$ and $LiZr_6Cl_{14}Mn$ to confirm the stoichiometries and to explain a puzzling lattice expansion trend found in the $A^1Zr_6Cl_{14}Mn$ series (Table 1). Some summary data are given in Table 2. Crystals of $Zr_6Cl_{14}Fe$ were not obtained in the syntheses described above, but small ones were found after a reaction at 750°C, followed by slow cooling, that was loaded to make "$NaZr_6Cl_{14}Fe$." Their lattice dimensions were essentially identical to those of $Zr_6Cl_{14}Fe$, making it improbable that the planned 19-electron cluster phase had formed. Following the same path, crystals of $LiZr_6Cl_{14}Mn$ (and $Li_2Zr_6Cl_{15}Mn$ (8)) were obtained from an off-stoichiometry reaction designed to produce the latter (950/800°C gradient). The total yield of both cluster phases was no higher than 40%.

Structure Determinations

Intensity data for $Zr_6Cl_{14}Fe$ were collected on a SYNTEX diffractometer. The observed diffraction intensities were low because of the small size of the crystal, the intrinsic properties of the structure that result in a small number of strong reflections, and the limited power of the incident beam. A thirty-minute rotation photo on the diffractometer barely gave enough reflections to determine the orientation matrix, the accuracy of which was then improved by replacement of the lower angle reflections with higher ones. Axial photographs for both the primitive monoclinic cell found and its orthorhombic transformation confirmed the *mmm* Laue symmetry of the latter that was expected on the basis of the powder pattern. Data from two octants with $2\theta < 55°$ were collected with variable scan rates of 2.02° to 19.53° per min. Empirical θ-dependent absorption corrections were applied to the raw data based on three ψ-scans at approximately 15, 25, and 40° in 2θ. The data set was then reduced and averaged in space group *Cmca* after the appropriate absence conditions were confirmed. Positions of zirconium and chlorine atoms in $Zr_6Cl_{14}C$ (3) were used as the starting model, and an electron difference map after isotropic refinements ($R = 0.161$) showed a residue of about 10 $e^-/Å^3$ at the center of the zirconium cluster. Addition of iron at that point and isotropic refinement gave $R = 0.071$, $R_w = 0.116$. Difference maps calculated before and after anisotropic refinement were essentially flat except a few ghost peaks of 0.6 $e^-/Å^3$ around Cl5, indicating the absence of sodium in the structure. No significant variation of the iron occupancy from unity (102(2)%) was observed.

Study of $LiZr_6Cl_{14}Mn$ diffraction was conducted on a CAD4 diffractometer. Axial photos about the three principal axes and the [110] direction confirmed the C-centered orthorhombic cell. Two octants of data were collected up to $2\theta = 60°$ with the centering condition $h + k = 2n$. Two additional independent reflection conditions found in the data implied the space groups *Cc2a* or *Ccmb* (nonstandard settings), and the latter was chosen and transformed to the standard setting *Cmca* to match that of the parent compound Nb_6Cl_{14} (12). The diffraction data were corrected for nonlinear decay (4.1% in 35.9 hr) since the three intensity standards decreased at rather different rates, and an empirical absorption correction was applied through the use of 10 ψ-scans. The reduced data set was averaged both for reflections with $I > 0$ (2768 in number) and for those with $I > 3\sigma_I$(1864). The structure excluding Li was refined with 883 independent observed data starting with $Zr_6Cl_{14}Fe$ as the model and quickly converged at $R = 4.1\%$, $R_w = 5.3\%$.

A Li^+ countercation was expected in the lattice according to the cluster electron counting rules, the starting composition, and the distinctive lattice constants. A dif-

TABLE 2
Some Data Collection and Refinement Parameters

	$Zr_6Cl_{14}Fe$	$LiZr_6Cl_{14}Mn$
Space group, Z	Cmca (no. 64), 4	Cmca (No. 64), 4
Crystal dimen., mm	0.10 × 0.09 × 0.05	0.22 × 0.24 × 0.24
Data collection instrument	SYNTEX $P2_1$	CAD-4
Scan mode	ω	ω
$2\theta_{max}$, deg.	55	60
Octants meas.	$\pm h, k, l$	$h, k, \pm l$
Refl. meas.	2723	3414
Obs.	778 ($I > 3\sigma_I$)	2768 ($I > 0$), 1864 ($I > 3\sigma_I$)
Indep.	489	1350, 883
Abs. coeff. (Mo$K\alpha$), cm^{-1}	51.5	55.2
Range of transm. coeff.	0.543–0.721	0.88–1.00
R_{ave}, % (obs. data)	4.7	5.1
Second. ext. coeff.	$1.2(8) \times 10^{-5}$	$6(2) \times 10^{-8}$
Variables	54	59
R,[a]%	5.5	6.8
R_w,[b]%	5.5	5.3
largest residue peak, $e^-/Å^3$	0.6	+1.6 (0.48 Å from Zr1) −1.7 (0.69 Å from Mn)

[a] $R = \Sigma||F_o| - |F_c||/\Sigma|F_o|$.
[b] $R_w = [\Sigma w(|F_o| - |F_c|)^2/\Sigma w(F_o)^2]^{1/2}$; $w = \sigma_F^{-2}$.

ference Fourier map calculated with all data indicated that the refined position of the countercation in $CsZr_6I_{14}C$ was clean; instead, a 1.9 $e^-/Å^3$ residue was found in an interstice surrounded by six chlorines. The converged refinement of the thermal parameter and multiplicity of Li at this position gave reasonable occupancy of 25.2(2)% for each of the 16 symmetry-related positions, corresponding to one cation per cluster. The isotropic thermal parameter for Li and the Li–Cl distances were also plausible. The alternative anisotropic refinement of all heavy atoms with data averaged with a 3σ cut-off gave a rather flat difference Fourier map, with the highest positive residue being a ghost peak of 1.3 $e^-/Å^3$ near Zr2. However, there were also two peaks of comparable size close to the Li position found with the aid of the weak data (above). The ultimate structure refinement with these data was essentially the same as that refined with all reflections with $I > 0$, indicating that the weaker reflections helped to locate the light Li atom but did not contribute significantly to the final results. The standard deviations of parameters were slightly higher with fewer observations.

Refinement of the Mn occupancy with either averaged data set gave 90.0(4)% and a shrinkage of its thermal parameters together with a reduction of the negative ghost peaks around Mn. Based on the arguments presented before (10), such a result at a point of high symmetry was considered to derive from imperfect crystallographic data rather than a true defect at this position. Full occupancy caused a slight increase of the negative residue around Mn from −1.3 $e^-/Å^3$ to −1.6 $e^-/Å^3$.

The final difference map was essentially flat, showing ghost peaks around Zr1, Zr2, and Mn. However, there was a residue of 1.0 $e^-/Å^3$ at the origin of the unit cell, which corresponds to the cation position in $CsZr_6I_{14}C$. Refinement of a second Li atom there failed as indicated by an unreasonably large B_{iso}.

^7Li NMR Spectra

These were measured on a static sample at room temperature with the aid of a Bruker WM-200 instrument and solid LiCl as the reference. This sample was prepared by allowing stoichiometric amounts of starting materials to react at 750°C for 20 days followed by an annealing at 580°C for 20 days. The product was a black powder free of impurities detectable by X-ray diffraction. A 50 mg sample was sealed in Pyrex tubing under nitrogen.

RESULTS AND DISCUSSION

The positional parameters and isotropic displacement equivalents for $Zr_6Cl_{14}Fe$ and $LiZr_6Cl_{14}Mn$ are given in Table 3 while the more important distances appear in Table 4. Anisotropic displacement data and F_o/F_c listings are available from J. D. C.

The structure frameworks in $Zr_6Cl_{14}Fe$ and $LiZr_6Cl_{14}Mn$, Fig. 1, are essentially identical to that of the parent compound Nb_6Cl_{14} except for the interstitial atom Fe or Mn and the cation, if any. The three-dimensional cluster network can be described as $[Zr_6(Z)Cl^i_{10}Cl^{i-a}_{2/2}]Cl^{a-i}_{4/2}Cl^{a-i}_{2/2}$, where i and a denote the metal

TABLE 3
Positional and Thermal Parameters for $Zr_6Cl_{14}Fe$ and $LiZr_6Cl_{14}Mn$

	x	y	z	B_{eq}^a
		$Zr_6Cl_{14}Fe$		
Zr1	0.3778(1)	0.0739(2)	0.8805(2)	0.83(8)
Zr2	0	0.3440(3)	0.8877(4)	0.8(1)
Cl1	0.1231(6)	0.0866(4)	0.2517(6)	1.4(3)
Cl2	0.1240(6)	0.2548(6)	0.0073(6)	1.4(2)
Cl3	¼	0.342(1)	¼	1.5(3)
Cl4	0	0.157(1)	0.758(1)	1.3(4)
Cl5	0.2472(6)	0	0	1.5(4)
Fe	0	0	½	0.7(3)
		$LiZr_6Cl_{14}Mn$		
Zr1	0.38093(5)	0.07327(5)	0.88124(6)	1.38(1)
Zr2	0	0.34636(8)	0.88801(9)	1.40(2)
Cl1	0.1234(1)	0.0870(1)	0.2503(2)	1.83(3)
Cl2	0.1239(1)	0.2557(2)	0.0063(2)	1.81(3)
Cl3	¼	0.3411(2)	¼	1.99(5)
Cl4	0	0.1576(2)	0.7600(2)	1.90(5)
Cl5	0.2491(2)	0	0	1.79(4)
Mn	0	0	½	1.81(4)
Li[b]	0.251(4)	0.676(4)	0.153(5)	1.9(8)

[a] $B_{eq} = (8\pi^2/3)\Sigma_i\Sigma_j U_{ij} a_i^* a_j^* \mathbf{a}_i \mathbf{a}_j$.
[b] Occupancy = 25.2(2)%.

edge and exo (intercluster) bonding functions of halide, respectively. The Li^+ countercation in $LiZr_6Cl_{14}Mn$ occupies a distorted chlorine octahedral interstice between clusters, Fig. 2.

As in all examples of this particular network (3, 12, 13), the cluster cores with Fe and Mn interstitials undergo a tetragonal distortion such that the two types of Zr–Mn and Zr–Fe distances differ by ~2%, 0.039 Å and 0.046 Å, respectively. This can be explained as a result of a asymmetric nature of the terminal exo chlorine atoms, the closer and presumably stronger Zr1–Cl^{a-a} exo bonding being *trans* to the longer Zr1–Z. However, the 0.08 and 0.11 Å differences in Zr1–Zr1 distances that result here (the horizontal and vertical separations as shown in Fig. 1) are strikingly greater than the 0.04 Å differences observed in the carbon- and boron-centered zirconium chloride clusters (13). Why this difference should be more pronounced in the 3*d*-metal-centered compounds is not obvious. It could be the result of the difference in the electronic structure between 14 e^- and 18e^- clusters, where t_{1u} (*p*) has been replaced by t_{2g} (*d*) in the bonding orbitals used by Z or the consequence of cluster expansion by over 0.1 Å or both. Otherwise, these clusters behave rather normally in the sense that the average Zr–Fe and Zr–Mn distances agree with those in other related cluster phases, e.g., $LiZr_6Cl_{15}Fe$ (8), 2.424(1) Å; $KZr_6Cl_{15}Fe$ (15), 2.423 Å (ave), $Li_2Zr_6Cl_{15}Mn$ (8), 2.4111(6) Å; $Cs_3(ZrCl_5)Zr_6Cl_{15}Mn$ (15), 2.4142(4) Å. A smaller cluster core is regularly observed for manganese. Similar to what is observed in the analogous iodide systems, a lengthening of the Zr–X^i distances accompanies a decrease in cluster core size, perhaps because of a matrix effect. At the same time, the lattice of $Zr_6Cl_{14}Mn$ is expanded by incorporation of the countercation Li^+, and this also results in the stretching of the Zr–Cl^a distances via Li–Cl^a interactions (2).

The location of the countercation in $LiZr_6Cl_{14}Mn$ is also novel. In contrast to the larger monovalent cations, which occupy a 12-coordinate position in the close-packed layers (0, 0, 0, etc. in Fig. 1) with a centroid–Cl distance of ~3.64 Å, the smaller Li^+ is bound in a distorted octahedral interstice between close-packed chlorine layers, Fig. 2, with $\bar{d}$ = 2.61 Å. The Li–Cl distance is slightly but probably not significantly greater than the sum of Cl^- and six-coordinate Li^+ crystal radii, 2.57 Å (16), presumably because the site is in fact occupied only 25% of the time. The lithium is not located at the center of the interstice either but closer to one of the triangular faces, resulting

TABLE 4
Important Distances and Angles in $Zr_6Cl_{14}Fe$ and $LiZr_6Cl_{14}Mn$

		$Zr_6Cl_{14}Fe$	$LiZr_6Cl_{14}Mn$
		Distances (Å)	
Zr1–Z	×4	2.438(2)	2.4147(7)
Zr2–Z	×2	2.392(4)	2.376(1)
$\bar{d}$		2.423	2.402
Zr1–Zr1	×2	3.390(5)	3.375(1)
	×2	3.503(4)	3.455(1)
Zr–Zr2	×4	3.420(4)	3.384(1)
	×4	3.410(5)	3.392(1)
$\bar{d}$		3.246	3.397
Zr1–$Cl5^i$	×4	2.526(7)	2.551(2)
Zr1–$Cl1^i$	×4	2.557(8)	2.576(2)
Zr1–$Cl2^i$	×4	2.552(7)	2.568(2)
Zr2–$Cl1^i$	×4	2.544(9)	2.564(2)
Zr2–$Cl2^i$	×4	2.539(8)	2.556(2)
$\bar{d}$		2.544	2.563
Zr1–$Cl4^{i-a}$	×4	2.62(1)	2.633(2)
Zr2–$Cl4^{a-i}$	×2	2.84(2)	2.857(3)
Zr1–$Cl3^{a-a}$	×4	2.624(7)	2.685(1)
Li–$Cl1^i$			2.44(6)
			2.45(6)
Li–$Cl2^i$			2.78(6)
			2.71(6)
Li–$Cl3^a$			2.41(5)
Li–$Cl5^i$			2.89(5)
$\bar{d}$			2.61
		Angles (°)	
Cl1–Zr1–2	×4		173.54(7)
Cl4–Zr1–Cl5	×4		172.39(6)
Cl1–Zr2–Cl2	×4		171.38(8)
average			172.4

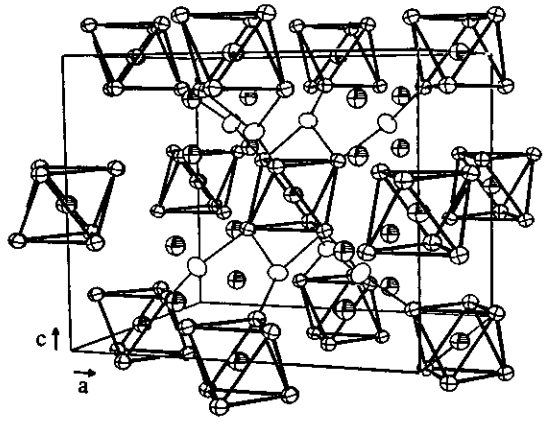

FIG. 1. The metal clusters, the intercluster halogen bridging to the central unit, and the Li^+ positions in the structure of $LiZr_6Cl_{14}Mn$ (90% probability ellipsoids). Li and Mn, Zr and Cl are depicted by shaded, crossed, and open ellipsoids, respectively. The 10 chlorine atoms on each metal cluster that only bridge edges have been omitted for clarity. Zr2 and the $Cl4^{a-i}$ atoms that are bonded exo to Zr2 lie on the mirror plane at $\frac{1}{4}$, y, z. The $Cl3^{a-a}$ atoms shown bridge at four Zr1 vertices on each cluster.

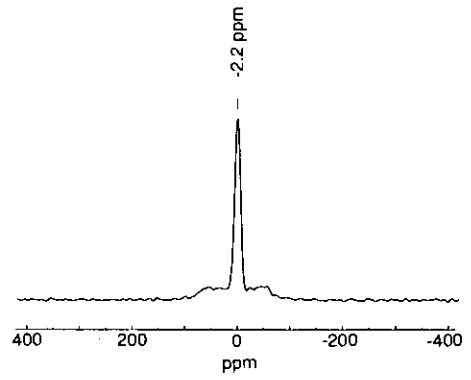

FIG. 3. The static ^7Li NMR spectrum of $LiZr_6Cl_{14}Mn(s)$ at room temperature relative to that of $LiCl(s)$.

in three short and three long Li–Cl distances (upward in Fig. 2). The displacement of Li by about 0.3 Å is not surprising when the size of the vacancy and the positioning of the surrounding cluster units are taken into consideration. Somewhat positive zirconium atoms reside between the same pair of Cl layers as does Li and at rather close distances (<3.76 Å), while the Zr atoms on the other side are farther away (>3.96 Å). This behavior is helpful in understanding the quadrupole coupling constant of ^7Li in this phase, which is smaller than that in $Li_2Zr_6Cl_{15}Mn$.

^7Li Solid State NMR for $LiZr_6Cl_{14}Mn$

To provide evidence in support of the results of the single crystal study, ^7Li solid state NMR experiments were also conducted on $LiZr_6Cl_{14}Mn$. The spectrum, Fig. 3, contains a sharp central peak and two rather featureless side bands. The fact that only one signal is observed is consistent with the structural analysis which revealed only one type of Li position. The line shape is distinctly different from that of LiCl, which gives a typical Gaussian peak, and this confirms the existence of the cation in a position with symmetry lower than cubic. The chemical shift of the signal with respect to LiCl, −2.2 ppm, is rather small compared with +11.6 ppm in $Li_6Zr_6Cl_{18}H$ (9) and indicates more similar chemical environments in $LiZr_6Cl_{14}Mn$ and LiCl, that is, in the number of Cl atoms around the Li and the charge distributions between Li and Cl. (The Li in the paramagnetic $Li_6Zr_6Cl_{18}H$ has three of the more basic Cl^a atoms as neighbors.) The ill-defined side-band profiles found here presumably are associated with a poor crystallinity of the sample which was prepared at a relatively low temperature. In addition, instrumental limitations made it difficult to locate the centers of the side bands and thence impossible to determine the asymmetric parameter (η) and the quadrupole coupling constant (Q_c) with accuracy. Nevertheless, the less distinctive side bands compared with those in $Li_2Zr_6Cl_{15}Mn$ (8), where Li lies on a site of D_{2d} symmetry, imply a symmetry lower than axial ($\eta > 0$), in agreement with the diffraction evidence that Li sits on a general position ($\eta \neq 0$). Furthermore, the line profile of this spectrum is certainly different from that for $\eta = 1$, which has washed-out singlets and shoulders and is essentially one broad central peak (17). Although the Li site does not have a well-defined axial symmetry, the three short and three long Li–Cl distances yield a pseudo-threefold axis along **c**, so η is expected to be not too far away from zero. Assuming η is close to 0, one can estimate Q_c to be smaller than, but in the vicinity of, 14 kHz by assigning the edges of the side-bands as singlets at ±60 ppm ($\gamma_1 = Q_c = 120$ ppm, 14 kHz). The small value of Q_c compared with 58 kHz in $Li_2Zr_6Cl_{15}Mn$ is not understood yet; it is probably associated with the lower occupancy (25% vs 33%), lower symmetry, and the three long Li–Cl distances in this compound. The ^7Li NMR results in any case support the fact that Li is in the

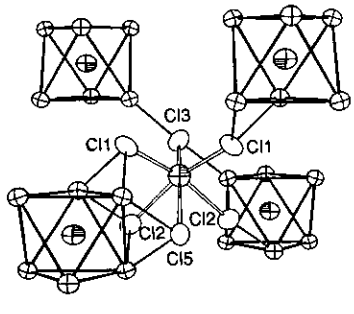

FIG. 2. The chlorine environment around lithium in $LiZr_6Cl_{14}Mn$ (90%). All other chlorine atoms have been left out.

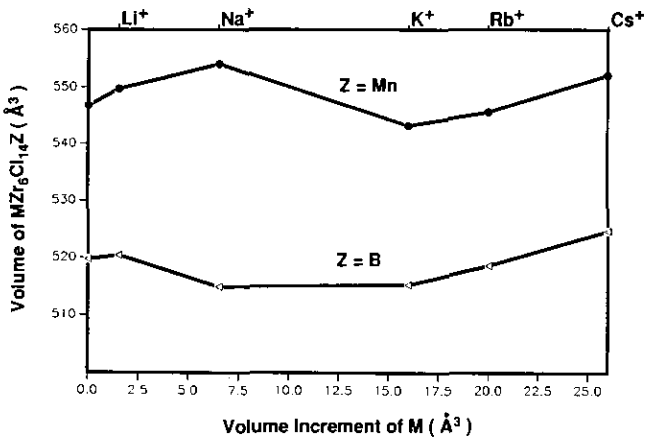

FIG. 4. The unit cell volumes of $A^1Zr_6Cl_{14}Z$ as a function of the volumes of A^+ (Å^3 from Biltz (18)). The volume data for Z = B are taken from (13). Cations in $NaZr_6Cl_{14}Mn$ and $LiZr_6Cl_{14}B$ are assigned on this basis to the six-coordinate site found in $LiZr_6Cl_{14}Mn$.

lattice and agree with the symmetry of the refined position.

Structural Variations in the $MZr_6Cl_{14}Z$ Series

Ziebarth recognized that the cell volume of $LiZr_6Cl_{14}B$ does not fit into the volume trend of the other $AZr_6Cl_{14}B$ compounds even though it also has a 14 cluster-electron count (13). Similarly irregular lattice expansions are observed for the $AZr_6Cl_{14}Mn$ series (Table I) and, based on experience, such phenomena usually imply structural modifications. The present study establishes that $LiZr_6Cl_{14}Mn$ affords a second modification of the original Nb_6Cl_{14} structure. While a large cation as in $CsZr_6I_{14}C$ (3) has 12 chlorine neighbors, the smaller lithium disorders over four times as many six-coordinate positions. With this information, discontinuities in the cell volume vs countercation volume found for $AZr_6Cl_{14}Z$ for both Z = B and Fe, Fig. 4, can be rationalized. Although the cation-free $Zr_6Cl_{14}Mn$ and $Zr_6Cl_{14}B$ are 17- and 13-electron cluster phases, respectively, they still afford helpful references for the cation-free systems as long as we remember that a lattice expansion owing to the oxidation of the cluster core will be present, this usually being less profound than those caused by cation variations. In fact, this expansion will result in an understatement of the effect that lithium insertion has on cell volume.

For the Mn series, Li^+, and apparently Na^+ based on its cell volume, choose the six-coordinate position, presumably because the alternative 12-coordinate position is too large to provide sufficient cation–anion interactions. With r_{Cl} = 1.79 Å, one-half of the average nearest-neighbor Cl · · · Cl distance in $LiZr_6Cl_{14}Mn$, the average six-coordinate interstice is smaller than that expected necessary on the basis of standard crystal radii (16). The incorporation of these cations thus enlarges the interstice and therefore the lattice with respect to $Zr_6Cl_{14}Mn$. As r_+/r_- increases, the CN = 6 position becomes less favorable compared with the CN = 12 site, and the K, Rb and Cs compounds adopt the latter $CsZr_6I_{14}C$ structure judging from the clearly diminished cell volumes, whereas Na^+ would "rattle" in this cavity. The interaction between cations and the chlorine atoms when $r_+/r_- < 1$ tends to pull the Cl atoms closer to certain extent, resulting a net volume decrease with respect to $Zr_6Cl_{14}Mn$, while Cs^+ with $r_+/r_- > 1$ induces a lattice expansion, as expected.

A similar trend in volume for the boride series can now be understood as well, the discontinuity now occurring between $LiZr_6Cl_{14}B$ and $NaZr_6Cl_{14}B$. The turning point for the structure type change from the $LiZr_6Cl_{14}Mn$ to the $CsZr_6I_{14}C$ type occurs here for Na^+, the new break-point in cation size clearly being associated with the smaller cluster core.

Additional evidence for the cation assignments just made on the basis of the peculiar volume changes in these series was obtained from powder pattern intensities. Switching cations between the large and small sites causes obvious intensity changes for some reflections in the low angle region of calculated powder patterns, especially for the heavier alkali metals (K, Rb, Cs). Such comparisons all support the assignment of these three alkali metals to the 12-coordinate position. On the other hand, an unambiguous judgment of the structure types for the lighter alkali metals, Li and Na, can not be made on the basis of the powder pattern intensities because of their smaller diffracting power.

The observed structure modifications in the $AZr_6Cl_{14}Z$ series present another example of a delicate balance between bonding interactions and space-filling efficiency. In these groups of compounds, cation–anion interactions are the generally dominant factor with respect to space-filling requirements. For smaller alkali metals, the choice of the cation position allows better coulombic interactions at the cost of lower space-filling efficiency. As the size of the cation becomes larger, a different cation position is selected by the heavier alkali metals that provides both sufficient cation–anion interactions and higher density materials. The shift from red to blue in the visible colors of these compounds with change of Z from B to Fe has been well accounted for by Bond and Hughbanks in terms of predicted differences in their MO states (19).

ACKNOWLEDGMENTS

The first $Zr_6Cl_{14}Mn$, $KZr_6Cl_{14}Mn$, and $CsZr_6Cl_{14}Mn$ samples were synthesized by Tim Hughbanks. This research was supported by the National Science Foundation, Solid State Chemistry, via Grant DMR-8902954. The work was performed in the Ames Laboratory, U.S. Department of Energy.

REFERENCES

1. R. P. Ziebarth and J. D. Corbett, *Acc. Chem. Res.* **22,** 256 (1989).
2. J. D. Corbett *in* "Modern Perspectives in Inorganic Crystal Chemistry" (E. Parthé, Ed.), NATO ASI Series C, pp. 27–56. Kluwer Academic, Dordrecht, The Netherlands, 1992.
3. J. D. Smith and J. D. Corbett, *J. Am. Chem. Soc.* **107,** 5704, (1985).
4. J. D. Smith and J. D. Corbett, *J. Am. Chem. Soc.* **108,** 1927 (1986).
5. T. Hughbanks, G. Rosenthal, and J. D. Corbett, *J. Am. Chem. Soc.* **110,** 1511 (1988).
6. T. Hughbanks, *Prog. Solid St. Chem.* **19,** 329 (1989).
7. J. Zhang and J. D. Corbett, *J. Less-Common Met.* **156,** 49 (1989).
8. J. Zhang and J. D. Corbett, *Inorg. Chem.* **30,** 431 (1991).
9. J. Zhang, R. P. Ziebarth, and J. D. Corbett, *Inorg. Chem.* **31,** 614 (1992).
10. J. Zhang and J. D. Corbett, *Inorg. Chem.* **32,** 1566 (1993).
11. R.-Y. Qi and J. D. Corbett, unpublished research.
12. A. Simon, H.-G. Von Schnering, H. Wöhrle, and H. Schäfer, *Z. Anorg. Allg. Chem.* **339,** 155 (1965).
13. R. P. Ziebarth and J. D. Corbett, *J. Solid State Chem.* **80,** 56 (1989).
14. R. P. Ziebarth, and J. D. Corbett *J. Am. Chem. Soc.* **107,** 4571 (1985).
15. J. Zhang and J. D. Corbett, unpublished research.
16. R. P. Shannon, *Acta Crystallogr. Sect. A* **32,** 751 (1976).
17. R. B. Crell and R. G. Barnes, *J. Chem. Phys.* **56,** 1549 (1972).
18. W. Biltz, "Raumchemie der festen Stoffe," p. 238. Verlag Voss, Leipzig, 1934.
19. M. R. Bond and T. Hughbanks, *Inorg. Chem.* **31,** 5015 (1992).